A LES Study of Wake Dynamics Control using Upstream Plasma Actuation on a Square Cylinder with Rounded Leading Edges

Journal of Physics: Conference Series **3173** (2026) 012044 doi:10.1088/1742-6596/3173/1/012044

A LES Study of Wake Dynamics Control using Upstream Plasma Actuation on a Square Cylinder with Rounded Leading Edges

Rithvik Magal[1,2], Gabriele Bellani[1,2], Alessandro Talamelli[1,2] and Guglielmo Minelli*[1,2]

[1]Dipartimento di Ingegneria Industriale, Università di Bologna, Forlì, Italy
[2]CIRI - Aerospace, Università di Bologna, Forlì, Italy

E-mail: guglielmo.minelli2@unibo.it

Abstract. The control of bluff-body wakes for reduced drag and enhanced stability has traditionally relied on the so-called direct-wake control approach. By the use of actuators or passive devices, one can manipulate the aerodynamic loads that act on the rear of the model. An alternative approach for the manipulation of the flow is to move the position of the actuator upstream, hence interacting with an easier-to-manipulate boundary layer. The present study will focus on a bluff-body flow solved via large-eddy simulations (LES) to investigate the effectiveness of an upstream plasma actuator (positioned at the leading edge) with regard to the manipulation of the wake dynamics and its aerodynamic loads. A rectangular cylinder with rounded leading edges, equipped with actuators positioned at the front curvatures is simulated at Re=40000. This geometry is representative of ground-vehicle configurations, such as truck cabs, and the present study highlights the potential of active flow control for such applications. The results show that sinusoidal actuation yields significantly greater performance than steady actuation. Both drag reduction and cross-flow load attenuation improve with increasing actuation frequency, up to a saturation point. A maximum drag reduction of approximately 40% is achieved in the optimal case.

1 Introduction

The aerodynamic performance of bluff bodies is highly correlated with their wake dynamics. In the case of bluff bodies, such as square cylinders with separation at the leading edge, the wake is characterised by a large separated region and the presence of vortex shedding. The large turbulent wake leads to reduced pressure levels at the base, thus leading to high drag force values. The periodic vortex shedding, on the other hand, in these geometries, leads to strong oscillations in the cross-flow force component. In these flow conditions, pressure drag is the major contributor ($\approx 85\%$) to total drag [1]. These aspects of aerodynamic behaviour are particularly important for ground transport applications such as trucks, buses and cars. In trucks alone, a reduction in drag coefficient of $0.15 - 0.25$ is estimated to provide fuel savings of 18000 litres per year per truck [2]. In ground vehicles closely resembling square cylinders, such as truck cabs, the front corners are rounded to mitigate flow separation and reduce drag but is not always sufficient (due to design or practical specification constraints such as pedestrian safety considerations) to avoid separation completely. Hence, square cylinders with rounded leading edges present a shape closely corresponding to ground vehicles and hence may be used as demonstrators to study the effectiveness of

flow control mechanisms.

Traditional approaches to controlling the wake dynamics of a bluff body have tried to directly control the large separated wake behind the bluff bodies, the so called *direct wake* control approach. The direct wake approach typically incurs a large control energy penalty, having to control a miss mass of large turbulent kinetic energy flow. An alternative approach implemented in this work, is a class of boundary layer control involving actuation on the fore-body, the so called *upstream actuation* control. The control effects in the case of upstream actuation propagate downstream and indirectly affect the wake structure downstream. This actuation strategy is characterised by a lower control energy level as compared to direct wake manipulation. The works of Minelli et. al. [3, 4, 5] show the applicability of active flow control, effected via blowing and suction jets, to the geometry considered for the present study.

Flow control techniques developed over the years are categorised as either passive or active. Passive flow control techniques do not require an energy input, some examples being vortex generators, flow vanes and slats. AFC (Active Flow Control) techniques, on the other hand, require an energy input in order to function, but are able to attain control authority generally not achievable with passive techniques. Some examples for AFC devices are suction or blowing actuators, synthetic jet actuators and plasma actuators. In particular, the subject of this work, Dialectric Barrier Discharge (DBD) plasma actuators distinguish themselves due to a series of characteristics such as lack of moving parts and limited intrusiveness in the flow, low weight, high frequency response and contained power consumption and price with respect to other types of actuators for active flow control. These actuators are made of two electrodes, one exposed to the flow and the other embedded between a dielectric material and the substrate. When an high voltage differential is applied between the two electrodes, local ionization of the air molecules occurs and plasma is formed over the exposed electrode. The ionized particles moves from the exposed electrode towards the covered one and the collision between the ionized species and the ambient air produces a electro-hydro-dynamic (EDH) force which acts as a flow control mechanism.

The applicability of DBD plasma actuators for active flow control for pressure drag reduction has been pursued as a research topic both numerically and by means of experiments. The effect of plasma actuation is numerically modelled as a body force source term in the momentum equation. Futrzynski et al. [6] performed LES of the flow around an half-cylinder using DBD plasma actuators, where, by using a single actuator, a drag reduction of up to 4.6% was achieved. By using a pair of consecutive actuators, however, a drag reduction of up to 10% was obtained. Chen et al. [7] experimentally tested the drag reduction capabilities over a D-shaped bluff body of different types of plasma actuator architectures. In fact, along with the classical DBD streamwise oriented plasma actuator, a set of Plasma Streamwise Vortex Generators (PSVGs) and a hybrid actuator of the DBD and PSVGs, were examined. The results showed a total drag reduction of approximately 10.3%, using the DBD actuator, while it was 12.1% and 13.9% for the PSVGs and hybrid actuator, respectively.

Studies of flow control strategies utilising DBD plasma actuators have also examined the effect of continuous and periodic actuation. When a plasma actuator is activated, the flow around the actuator is accelerated and a so-called "starting vortex" is formed. which subsequently propagates downstream and eventually becomes a self-similar structure in case of continuous actuation [8]. In the case of pulsed operation, where the actuator is periodically switched on and switched off, a train of vortices is instead observed [9]. Pulsed or periodic operation of plasma actuators are particularly applicable to flow separation control of laminar boundary layers and it is observed that the control efficiency depends on the ratio of the pulse frequency to the dominant flow frequencies [10]. It is observed that the efficacy of pulsed actuation with respect to steady actuation is valid even in the case of separating turbulent boundary layers in case of bluff bodies [11].

Flow control actuation strategies for wake control of bluff bodies using other actuation methods (blowing and suction jets, etc) have been multi-frequency periodic (sinusoidal) functions due to superior gains in drag reduction [12, 3]. However, there exists scarce evidence, both experimental and numerical, of sinusoidal actuation of plasma actuators.

This work hence seeks to investigate the action of spanwise-uniform DBD plasma actuation using the upstream control strategy applied at the rounded leading edge of a square cylinder for the purpose of drag reduction and control authority over the wake dynamics to reduce loads generated by the wake.

2 Methodology

Large Eddy Simulations (LES) were performed at $Re = 40000$ using the pimpleFoam incompressible finite volume Navier-Stokes solver available within OpenFOAM for resolving velocity and pressure fields. The front rounded corners have a curvature of $r = 0.05D$. The domain used for LES is shown in Fig. 1.

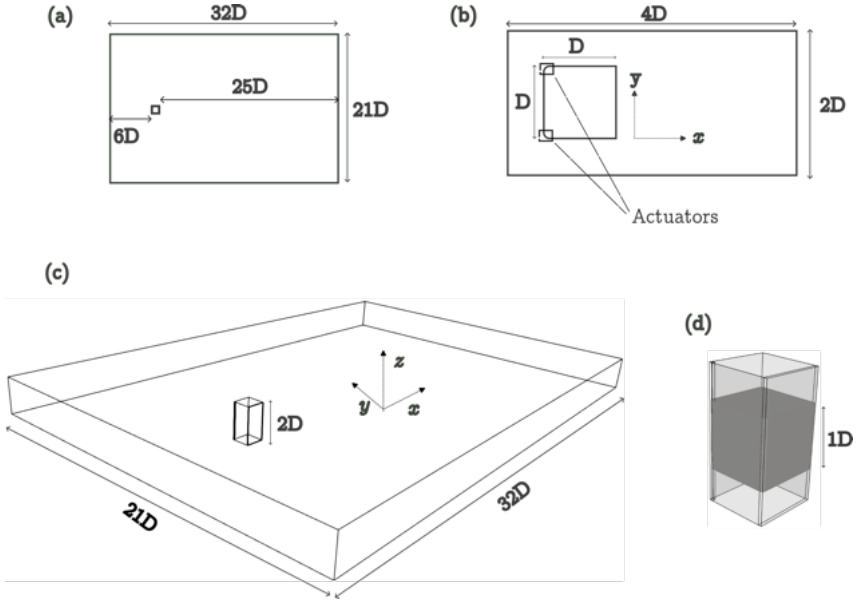

Figure 1: The domain used for the LES. (a) The domain dimensions. (b) A zoom of the sampling area for POD. (c) The 3-D domain. (d) A zoom of the 3-D extruded cylinder. A 3-D volume of 1D height is sampled throughout the simulation; the other two dimensions of the sampling volume are kept as in (b).

A constant velocity is imposed at the inlet and a constant homogenous pressure is imposed at the outlet. The value of the outlet pressure is inconsequential to the simulations due to the fact that an incompressible solver is used. The periodic boundary condition was applied to the spanwise extents of the domain (z-axis) while symmetry boundary condition was applied to the cross-stream extremities (y-axis).

2.1 Numerical Setup

The mesh is formed by hexahedral elements and the grid topology is constructed using a block mesh and the body-fitted technique in order to concentrate most of the elements close to the walls. The mesh spacing is derived from indications by Piomelli and Chasnov [13]. The wall-normal distance of the first grid point is located well within $y^+ = 1$ with $y^+ = u_T y/\nu$, where u_T is the friction velocity. The cell dimensions in the streamwise direction are maintained in the range $\Delta x^+ \approx 15 - 40$, where $\Delta x^+ = u_T \Delta x/\nu$ with $\Delta x^+ = 30$ in the mesh chosen after grid convergence studies. Similarly, the cell dimensions in the spanwise direction were considered in the range $\Delta z^+ \approx 50 - 150$, with the chosen mesh having $\Delta z^+ = 75$, where $\Delta z^+ = u_T \Delta z/\nu$. A grid independence study was further conducted to evaluate the influence of the spacing on the results.

A time step of $\Delta t^* = \Delta t U_\infty/D$ of $\Delta t^* = 3 \times 10^{-3}$ was used for all simulations. This resulted in a domain-averaged Courant-Freidrichs-Lewy (CFL) of ≈ 0.1 and a maximum CFL of ≈ 15 in localised zones near plasma actuation. All simulations were run for a flushing time $\Delta t^*_{flush} = t_{flush} U_\infty/D = 66$ (corresponding to 2 domain flow-throughs) followed by an averaging of $t^*_{averaging} = 132$, corresponding to 4 domain flow throughs. The second-order implicit Crank-Nicolson method was used for time marching. A central differencing second order scheme was used for the convective term. The wall-adapting local-eddy viscosity (WALE) [14] subgrid-scale model was used.

2.2 Plasma Actuator Modelling

The flow control effects of DBD plasma actuators are due to the electro-hydro-dynamic force (EHD force) generated due to collisions between charged particles (electrons and ions) with neutral surrounding air. Efforts to numerical model this phenomenon involve first principle models utilising the Boltzmann equation, and phenomenological models which estimate the EHD force from velocity field measurements [15]. Boltzmann equation models, while being the most accurate, require too high spatio-temporal resolutions for practical engineering studies. The two most popular phenomenological models, the Shyy and Suzen models, are hence found in the lion's share of existing literature involving flow control using DBD actuators.

Reynolds Averaged Navier-Stokes (RANS) simulations performed by Abdelraouf et al. [16] investigated the sensitivity of both Shyy [17] and Suzen [18] models on a NACA0012 airfoil. While both models produced near identical results in terms of lift gain and stall delay, the computational time using Suzen's model was 4 times greater. The similarity in performance between both these models is also reported by Bernal-Orozco et. al. [15] where the authors report negligible differences in the effect of the induced wall jet even in spite of differences in the calculated total body force.

The Shyy [17] body force model was used in this work to model the effect of plasma induced EHD force. The model assumes a linear variation of electric field and is an algebraic system compared to other models which require solving systems of partial differential equations. The Shyy model while being computationally affordable produces results comparable to higher fidelity models that solve Maxwell's equations for the electric field.

The Shyy model implements a linear variation of the electric field (refer Fig.2) in space via spatial gradients k_1 and k_2 along two cardinal axes x and y as:

$$|E| = E_0 - k_1 x - k_2 y \tag{1}$$

in which E_0 can be expressed as $E_0 = \frac{V}{d}$ with d being the separation between the two electrodes and V being the peak supply voltage. The gradients k_1 and k_2 can be evaluated using the condition that the field strength is the breakdown value at the plasma–fluid boundary (dimensions a and b). Hence, the gradients are:

$$k_1 = \frac{E_0 - E_b}{b}, \quad k_2 = \frac{E_0 - E_b}{a} \tag{2}$$

The body force F may hence be evaluated as:

$$F = E \rho_c e_c f_{supply}, \tag{3}$$

where ρ_c and e_c represent electron charge density and elementary charge respectively, and f_{supply} is the frequency of alternation of the supply voltage.

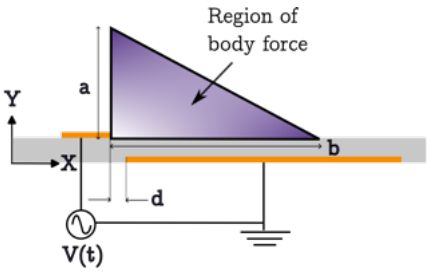

Figure 2: Schematic of the body force distribution using the Shyy model and the associated physical parameters.

A body force solver was developed implementing the Shyy model and interfacing with the pimpleFoam incompressible Navier-Stokes solver within OpenFOAM v2312 to introduce the body forces generated from plasma actuation as a forcing term in the momentum equation.

2.3 Plasma Actuator Characterisation

Simulations were carried out on a flat plate geometry with no surrounding flow to define the electrical parameters required to induce an ionic wind equal in magnitude to the inlet freestream velocity. A constant operating voltage of $5.7kV$ was chosen in order to match the dimensions ($a = 1.5mm$ and $b = 3mm$) of the ionised region as per Shyy et al [17] and the operating frequency was varied in order to effect the induced flow. Fig.3 presents the maximum velocity in the domain as a function of the actuator supply frequency f_{supply}.

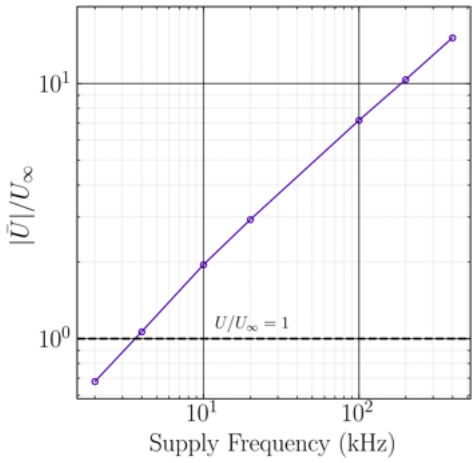

Figure 3: Maximum induced velocity magnitude obtained on application of the Shyy[17] model on a flat plate as a function of actuator supply frequency.

A supply frequency of $4kHz$ was consequently chosen as the operating point to induce a steady jet in which the maximum induced velocity was equal to the freestream velocity.

3 Results

3.1 Natural flow dynamics

Time-averaged wake topology, shown in Fig.4 for the case with no flow control action, presents an early pressure induced separation at the fore body, accompanied by a large side wake and a main wake. A wake closure distance of $\approx 1D$ is observed along with the presence of vortex cores, marked with red 'x' markers in Fig.4, representing the average position of the vortex shedding dynamics. It may be observed that while the position os the vortices in the side wake is symmetric, the vortices in the main wake show asymmetry of $\approx 0.1D$ in the stream-wise direction and $\approx 0.2D$ in the cross-stream direction. This minor asymmetry may be attributed to insufficiency of averaging time. It is observed from POD analysis (Fig 6b), that the interpretation of the flow physics is not affected by the averaging period used.

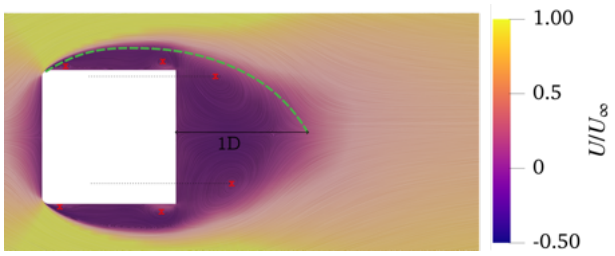

Figure 4: Line Integral Convolution (LIC) contour of time-averaged streamwise velocity normalised by the free-stream velocity for the no actuation case. Green dashed line represents the topology of the detached shear layer and red 'x' markers represent vortex cores.

The dynamics of the main wake is largely governed by vortex shedding. Fast Fourier Transform (FFT) applied to time-series of the drag (C_D) and lift (C_L) show peaks at $f \approx 0.1Hz$ that correspond to its regular shedding frequency, as shown in Fig.5.

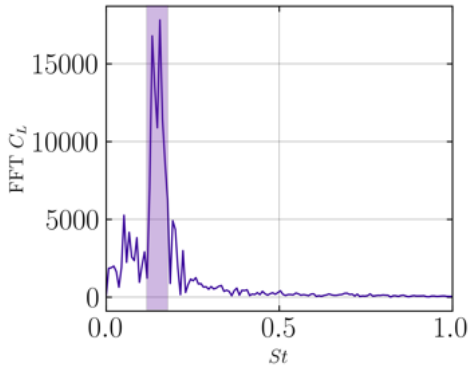

Figure 5: Fast Fourier Transform applied to time-series of the lift coefficient (C_L). The shaded region shows dominant peaks corresponding to vortex shedding frequency.

The predominance of vortex shedding over the wake dynamics is further evident on performing Proper Orthogonal Decomposition (POD) on the unactuated flow. POD was performed using the MODULO [19, 20] toolbox. POD results show that the most energetic mode pair corresponds to highly periodic vortex shedding, as demonstrated by the temporal coefficient evolution in Figs.6 b-c.

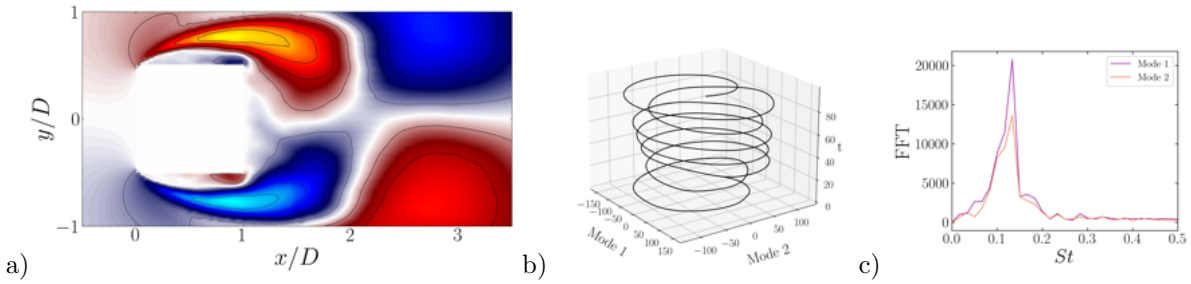

Figure 6: Vortex shedding mode pair corresponding to the unactuated case - a) structure, b) temporal coefficient evolution, and c) FFT of the temporal coefficients.

It is hence imperative that any eventual wake control action seeking to reduce drag must aim to reduce the coherence of the vortex shedding both in terms of spatial coherence and periodicity, thus suppressing the regular vortex shedding dynamics.

3.2 Flow control parameters

Two principal paramteres are considered for this study, viz. the positioning of the plasma actuator along the rounded leading edge, and the frequency of actuation, therefore implementing a time variation of the body force as $F(t) = |sin(2\pi f_{act} t)|$. A schematic of the considered parameter space is depicted in Figs.7a-b.

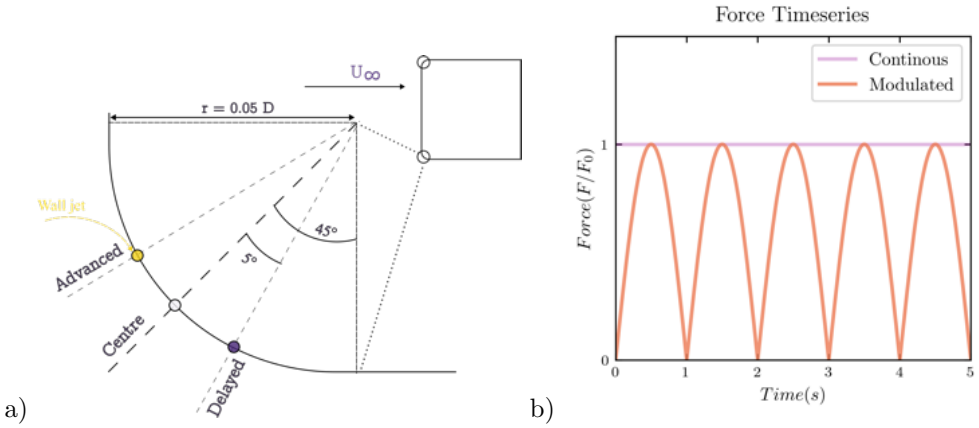

Figure 7: Parameter space for this study: a) The three actuator positions chosen for steady actuation and b) schematic showing the time evolution of the body force (source term for the momentum equation). The body force is normalised by the determined body force for continuous operation F_0 (refer Sec.2.3).

The uncontrolled flow shows separation at 45° of the leading edge curvature, marked 'Centre' in Fig.7a. Two positions azimuthally symmetric around the natural separation point were chosen to investigate the sensitivity to actuator positioning and the resulting drag reduction and reduction in lift oscillations with continuous plasma actuation is reported in Table 1.

Table 1: Reduction in drag and reduction in lift oscillations as a function of actuator position.

Position	Δ Coefficients (%)	
	ΔC_D	$\Delta std(C_L)$
Advance	-13.78	-12.29
Center	-9.13	-8.21
Delay	-18.13	-14.99

It is observed that actuating at the natural separation point provides the least gain both in terms of drag reduction as well as damping in lift oscillations. The best gain on both fronts is observed in the 'Delayed' position.

The 'Delayed' position (ref Fig.7a) was chosen for sinusoidal actuation. A sinusoidal forcing law of $F(t) = |sin(2\pi f_{act} t)|$ was utilised (ref Fig.7b). The reader is implored to separate the roles of the actuating frequency ($f_{act} = \mathcal{O}(1Hz)$) and the electrical supply frequency f_{supp} defined in Sec.2.3 ($f_{supp} = \mathcal{O}(1000Hz)$), the effect of f_{supp} being encapsulated within the body force calculation. The resulting drag reduction and reduction in the standard deviation of the lift coefficient are reported as a function of $St = f_{act} D/U_\infty$ in Fig.8.

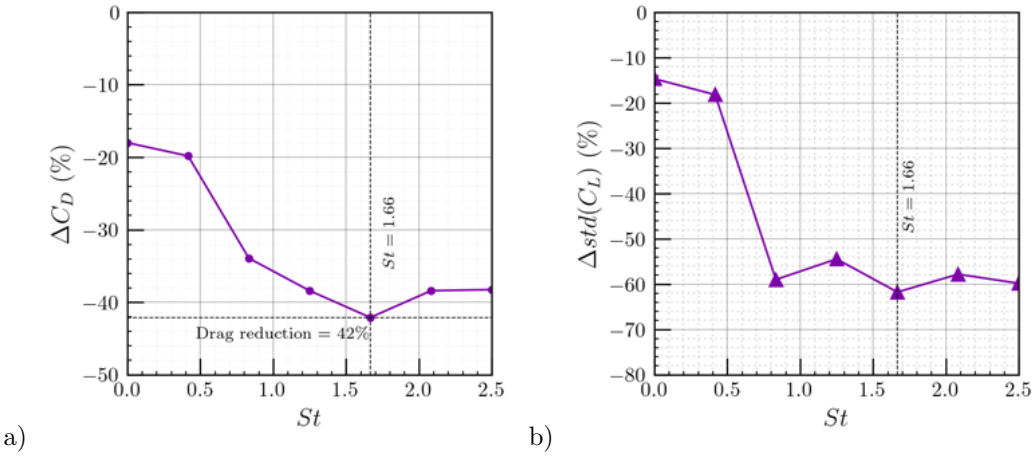

a) b)

Figure 8: a) Drag reduction in terms of ΔC_D and b) reduction in lift force oscillations in terms of $\Delta std(C_L)$ plotted as a function of actuation frequency of the body force.

It may be observed from Fig.8 that sinusoidal actuation provides better drag reduction as well as a higher level of damping of the lift oscillations. It is also observed that these gains reach a maximum at $St = 1.66$ and a plateau is observed with increasing actuation frequency.

3.3 Control Action

The unactuated case is compared to the best drag reduction case to glean an understanding of the modified wake dynamics and the propagation of the control action from the upstream position to the main wake through the side wake.

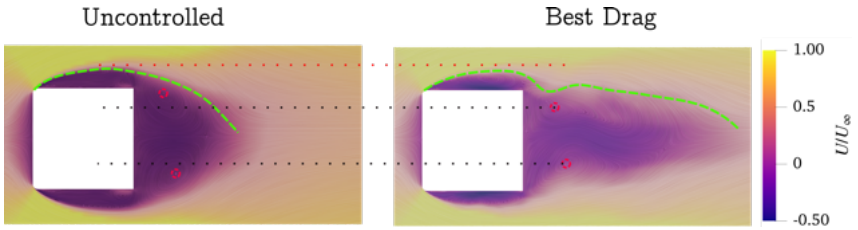

Figure 9: Line Integral Convolution (LIC) of time-averaged streamwise velocity normalised by the free-stream velocity for the unactuated case and best drag reduction case. Dashed lines in green show wake topology, dashed line in black show the contraction in vortex core positions and dashed line in red shows the reduction in side wake dimension.

It may be observed from Fig.9 that the average wake has been compacted in the cross-stream direction (evidenced by the relative positions of the red circles to the body) and has been stretched out in the streamwise direction with higher velocity values in the main wake, leading to higher base pressures.

The dynamic behaviour of the wake is captured via instantaneous minimum velocityy wake sensing as depicted in Fig.10 as scatterplots of instantaneous minimum velocity in the main wake across 5000 continuous snapshots which have been sampled at $100Hz$.

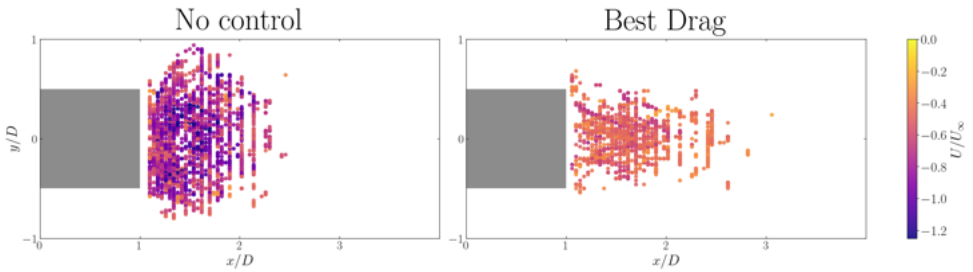

Figure 10: Scatter plots of instantaneous minimum streamwise velocity in the main wake across 5000 time steps for the unactuated case and best drag reduction case.

The control action may further be appreciated from the first POD mode pair for the best drag case, shown in Fig.11.

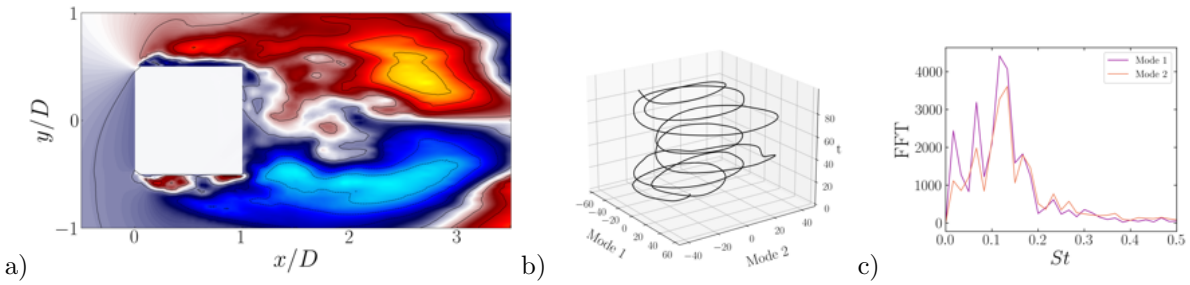

Figure 11: Vortex shedding mode pair corresponding to the best drag case - a) structure, b) temporal coefficient evolution, and c) FFT of the temporal coefficients.

In contrast to the unactuated modes shown in Fig.6, the spatial coherence of the shedding mode pair as well as their periodicity is found to be greatly reduced as a consequence of the control action.

The propagation of the control action from the leading edge through the side wake may be observed by considering FFT applied to the pressure timeseries at four streamwise stations within the respective detached shear layers (identified as the path along which $U/U_\infty = 1$). The purple line in Fig.12 corresponds to the shear layer of the unactuated case while the orange line corresponds to the shear layer of the best drag case characterised by a smaller side wake.

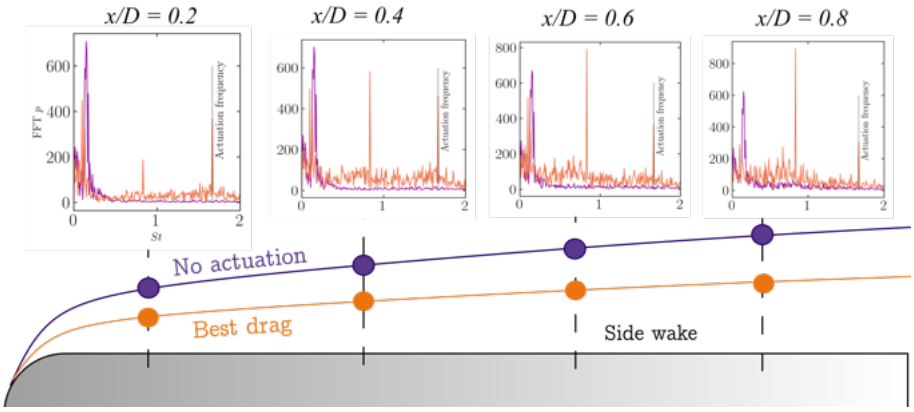

Figure 12: FFT applied to the pressure timeseries at points in the shear layer positioned at streamwise locations $x/D = 0.2$, $x/D = 0.4$, $x/D = 0.6$ and $x/D = 0.8$ at spanwise centre line $z/D = 1$.

The FFT plots of the unactuated flow shown in Fig.12 show a single dominant peak at $St \approx 0.1$, the vortex shedding frequency, present at all streamwise positions. The FFT plots instead of the best drag case show multiple distinct peaks: one at $St \approx 0.1$ corresponding to the vortex shedding, and other peaks corresponding to the body force actuation frequency and its harmonics. The continous damping of the vortex shedding peak observed with progressive downstream positions demonstrates that the upstream actuation suppresses the periodic vortex shedding dynamics. Furthermore, the peak corresponding to the actuation frequency is found to remain constant while the sub-harmonic peak ($St = 0.5\ St_{actuation}$) is found to increase in amplitude with downstream position and at positions after $0.5D$, this peak is observed to dominate the spectra.

The chosen actuated strategy of co-phase actuation, i.e synchronised actuation between the actuator pair also avoids the interference (that could be both constructive and destructive) that would be induced in the case of contra-phase actuation. Thus, the chosen actuation strategy tends to avoid any 'lock-in' effect with the vortex shedding phenomenon, rendering it robust across a range of actuation frequencies.

4 Conclusions

The Shyy model was implemented to model DBD plasma actuators positioned at rounded front edges of a square cylinder at $Re = 40000$. An optimal placement was determined for the actuators and a study was conducted to determine the optimal actuation strategy. Steady actuation was compared to time-varying actuation and the sinusoidal actuation was found to provide superior gains to steady actuation.

A reduction in drag of $\approx 40\%$ was obtained with a simultaneous reduction in the standard deviation of the lift (representing lift force oscillations) of $\approx 60\%$ actuating at $St = 1.66$. Principal component analysis via POD showed that the control action upstream affects the spatial coherence as well as the periodicity of vortex shedding, which is in fact the most energetic coherent structure for this flow case and is responsible to both drag and lift oscillations. The gains in aerodynamic performance were found to saturate at an actuation frequency corresponding to $St = 1.66$.

Finally, this work demonstrates the feasibility of DBD plasma actuators as an upstream actuated flow control device. The obtained drag reduction and control over wake dynamics are encouraging for further studies in optimising the multitude of control parameters such as the induced jet to freestream velocity ratio, orientation of the actuators and duty cycle and phase effects of time-varying actuation.

5 Acknowledgements

We acknowledge the CINECA award under the ISCRA initiative, for the availability of high performance computing resources and support.

References

[1] S. Ahmed, G. Ramm, and G. Faltin. Some salient features of the time-averaged ground vehicle wake. *SAE Technical Paper 840300*, 840300:A1, 2020.

[2] K. Cooper. Truck aerodynamics reborn - lessons from the past. In *SAE Technical Papers 2003-01-3376*, 11 2003.

[3] G. Minelli, T. Dong, B. R. Noack, and S. Krajnović. Upstream actuation for bluff-body wake control driven by a genetically inspired optimization. *Journal of Fluid Mechanics*, 893:A1, 2020.

[4] G. Minelli, M. Tokarev, J. Zhang, T. Liu, V. Chernoray, B. Basara, and S. Krajnović. Active aerodynamic control of a separated flow using streamwise synthetic jets. *Flow, Turbulence and Combustion*, 103, 11 2019.

[5] G. Minelli, E. Hartono, V. Chernoray, L. Hjelm, and S. Krajnović. Aerodynamic flow control for a generic truck cabin using synthetic jets. *Journal of Wind Engineering and Industrial Aerodynamics*, 168:81–90, 09 2017.

[6] R. Futrzynski. *Effect of drag reducing plasma actuators using LES*. PhD thesis, 2016.

[7] Z. Chen and C.Y. Wen. Flow control of a d-shaped bluff body using different dbd plasma actuators. *Journal of Fluids and Structures*, 103, 5 2021.

[8] R. Whalley and K.S. Choi. The starting vortex in quiescent air induced by dielectric-barrier-discharge plasma. *Journal of Fluid Mechanics*, 703, 07 2012.

[9] M. Kotsonis and S. Ghaemi. Experimental and numerical characterization of a plasma actuator in continuous and pulsed actuation. *Sensors and Actuators A: Physical*, 187:84–94, 2012.

[10] D. Greenblatt and I. Wygnanski. The control of flow separation by periodic excitation. *Progress in Aerospace Sciences - PROG AEROSP SCI*, 36:487–545, 10 2000.

[11] J. Vernet, R. Örlü, and P.H. Alfredsson. Flow separation control by dielectric barrier discharge plasma actuation via pulsed momentum injection. *AIP Advances*, 8:075229, 07 2018.

[12] Y. Li, C. Wenshi, J. Qing, Q. Li, Z. Yang, M. Morzynski, and B. Noack. Explorative gradient method for active drag reduction of the fluidic pinball and slanted ahmed body. *Journal of Fluid Mechanics*, 932, 02 2022.

[13] U. Piomelli and J. R. Chasnov. *Large-Eddy Simulations: Theory and Applications*, pages 269–336. Springer Netherlands, Dordrecht, 1996.

[14] N. Franck and F. Ducros. Subgrid-scale stress modelling based on the square of the velocity gradient tensor. *Flow Turbulence and Combustion*, 62:183–200, 09 1999.

[15] A. Bernal O., Raúl, I. Carvajal, and O. Huerta-Chavez. Performance of dbd actuator models under various operating parameters and modifications to improve them. *Fluids*, 8:112, 03 2023.

[16] H. Abdelraouf, A. Nagib, and S. Kassab. Simulations of flow separation control numerically using different plasma actuator models. *Alexandria Engineering Journal*, 59:3881–3896, 10 2020.

[17] B. Jayaraman and W. Shyy. Modeling of dielectric barrier discharge-induced fluid dynamics and heat transfer. *Progress in Aerospace Sciences*, 44(3):139–191, 2008.

[18] Y.B. Suzen and P.G. Huang. Simulations of flow separation control using plasma actuators. In *Collection of Technical Papers - 44th AIAA Aerospace Sciences Meeting*, volume 14, pages 10456–10464, 2006.

[19] R. Poletti, L. Schena, D. Ninni, and M.A. Mendez. Modulo: A python toolbox for data-driven modal decomposition. *Journal of Open Source Software*, 9(102):6753, 2024.

[20] D. Ninni and M.A. Mendez. Modulo: A software for multiscale proper orthogonal decomposition of data. *SoftwareX*, 12:100622, 2020.